THROUGHPUT OPTIMIZATION FOR NON-UNIFORM LINEAR ANTENNA ARRAYS IN MULTICELL WIMAX SYSTEMS

M. Nicoli [(1)]*, L. Sampietro* [(2)]*, C. Santacesaria* [(2)]*, S. Savazzi* [(1)]*, O. Simeone* [(1)(3)]*, U. Spagnolini* [(1)]

[(1)] Dipartimento di Elettronica e Informazione, Politecnico di Milano, Italy
[(2)] Siemens S.p.A. Com CRD MW, Cassina de' Pecchi (Milano), Italy
[(3)] CCSPR, New Jersey Institute of Technology (NJIT), Newark, USA
{nicoli,savazzi,simeone,spagnoli}@elet.polimi.it, {luigi.sampietro,claudio.santacesaria}@siemens.com

ABSTRACT

A WiMAX multi-cell system conforming the IEEE 802.16-2004 standard which supports multiple antennas and OFDM modulation is considered. Focusing on the uplink, we show that Signal to Interference plus Noise Ratio (SINR) degradation caused by fading impairments can be considerably reduced by exploiting adaptive modulation/coding techniques in conjunction with a non-uniform antenna array with optimized spacings. Specifically, a trade off between diversity gain and array interference reduction capability is considered so as to derive closed form solutions for the antenna spacings. Performance improvements are investigated by analyzing the cell coverage and the average throughput for various cellular plannings, antenna configurations and channel models. For completeness, SINR degradation due to shadowing effect is also considered.

1. INTRODUCTION

WiMAX (Worldwide Interoperability for Microwave Access) is a standard-based technology that provides fixed last mile broadband wireless access, intended as a cost-effective alternative to existing wired technologies such as cable and Digital Subscriber Line (DSL) [1]. In this paper, we consider WiMAX multi-cell systems conforming to the IEEE 802.16-2004 standard [2] [3], which prescribes the use of OFDM modulation and supports multiple antennas and adaptive modulation/coding. In the uplink of these systems, a major source of impairment is the degradation of the signal-to-interference-plus-noise-ratio (SINR) generated by multipath fading and out-of-cell interference (due to frequency reuse). The use of multiple antennas at the base station is known to reduce such effects by providing either diversity or beamforming gains, depending on the inter-element spacing of the array [8]. Diversity-oriented schemes use large antenna spacing to get fading uncorrelation and mitigate the impairments caused by channel fluctuations. On the other hand, when a small spacing is adopted, the fading is highly correlated and beamforming techniques may be employed for interference rejection. The optimal spacing is the one providing the best trade-off between diversity gain and interference rejection capability, depending on the specific propagation environment [4].

The contribution of this paper is twofold. At first, we deal with the optimization of the array deployment, formulated as the maximization of the average SINR at the output of a Minimum Variance Distortionless Response (MVDR) receiver [8]. Then, assuming the optimal array deployment at the BS, we evaluate the coverage and average throughput of the system, assessing the benefits of optimized antenna arrays with respect to conventional arrays under different assumptions for the cellular layout and propagation environment.

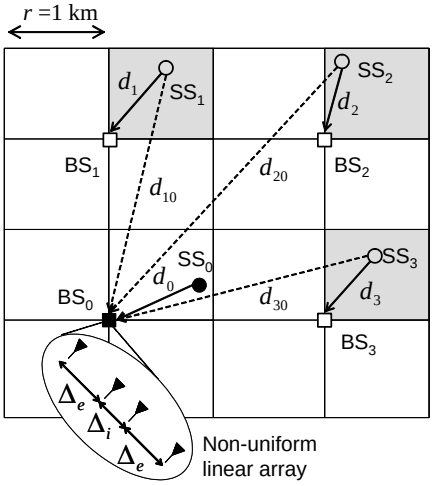

Fig. 1. Uplink layout for a wireless cellular system. Shaded cells represent the first ring of interference for reception of user SS_0 by base station BS_0.

2. SYSTEM AND SIGNAL MODEL

We consider the uplink of a IEEE 802.16-2004 compliant system [2] [3] with fixed subscriber stations. Fig. 1 exemplifies the scenario of interest for a square layout with cell side $r = 1$ km and frequency reuse factor $F = 4$. In this example, the transmission by the subscriber station SS_0 to its own base station BS_0 is impaired by the interference from $N_I = 3$ out-of-cell subscriber stations $\{SS_i\}_{i=1}^{N_I}$ that employ the same subcarrier frequencies. In the figure, d_i denotes the distance of the ith terminal from its base station for $i = 0, \cdots, N_I$, while d_{i0} is the distance of the interferer SS_i (with $i \neq 0$) from BS_0. The base station BS_0 is equipped with a linear symmetric array of M antennas, while SS's have a single antenna (either omnidirectional or directional). An example of symmetric array covering a 90 degree sector is shown in fig. 1 for $M = 4$, external antenna spacing Δ_e and internal spacing Δ_i.

The equivalent discrete-time baseband model for the transmitter is illustrated in fig. 2. The information-bearing sequence $\{b_i\}$ is coded by the concatenation of a Reed Solomon code and a convolutional code, it is bit interleaved and mapped into complex symbols $\{x_k\}$ belonging to the constellation of the selected digital modula-

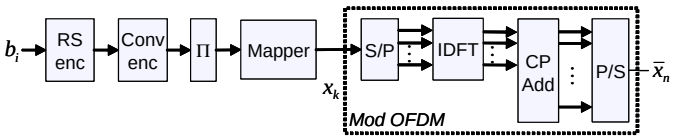

Fig. 2. Transmitter baseband model.

tion. According to the adaptive modulation and coding approach, the coding and modulation parameters are selected based on the channel state so as to guarantee a fixed bit error rate (BER= 10^{-6}): seven possible transmission modes $\{\mathrm{T}_i\}_{i=1}^{7}$ are prescribed by the standard [2] [3], as listed in Table 1. OFDM modulation is finally carried out using a N-point IDFT and a cyclic prefix of W samples.

At the receiver, OFDM demodulation is carried out at each receiving antenna as shown in fig. 3. The $M \times 1$ signal obtained at the output of the M demodulators on the kth subcarrier is modelled as

$$\mathbf{y}_k = [y_{1,k} \cdots y_{M,k}] = \mathbf{h}_k x_k + \mathbf{n}_k,$$

with $k = 1, \ldots, K$, and K denoting the number of useful subcarriers (the remaining $N - K$ are used as guard-band or DC subcarriers). The $M \times 1$ channel vector $\mathbf{h}_k$ gathers the M complex channel gains for the links between SS_0 and the antenna array at BS_0, while x_k denotes the symbol transmitted on the kth subcarrier with $E[|x_k|^2] = 1$. The $M \times 1$ vector $\mathbf{n}_k$, modelling both the background noise and the out-of-cell interference, is assumed to be zero-mean complex (circularly symmetric) Gaussian, temporally uncorrelated but spatially correlated with spatial covariance $\mathbf{Q} = \mathrm{E}[\mathbf{n}_k \mathbf{n}_k^{\mathrm{H}}]$.

As shown in fig. 4, the receiver consists of a space-frequency equalizer that performs MVDR [8] spatial filtering $\hat{x}_k = \mathbf{w}_k^{\mathrm{H}} \mathbf{y}_k$ on each subcarrier, with:

$$\mathbf{w}_k = \mathbf{Q}^{-1}\mathbf{h}_k \left(\mathbf{h}_k^{\mathrm{H}} \mathbf{Q}^{-1} \mathbf{h}_k\right)^{-1}. \quad (1)$$

It can be easily shown that the resulting signal-to-noise ratio (SNR) at the output is [8]:

$$\rho_k = \frac{\mathrm{E}\left[|x_k|^2\right]}{\mathrm{E}\left[|\hat{x}_k - x_k|^2\right]} = \mathbf{h}_k^{\mathrm{H}} \mathbf{Q}^{-1} \mathbf{h}_k. \quad (2)$$

The estimated symbols $\hat{x}_k$ are then used by the maximum-likelihood demodulator to compute the log-likelihood ratio (LLR) for each code bit. Finally, bit deinterleaving, bit maximum-a-posteriori (Log-MAP) convolutional decoding and RS decoding are performed to obtain the transmitted data estimate $\{\hat{b}_i\}$. Numerical values for the main system parameters used throughout the paper are listed in Table 1.

Table 1. Transmission modes from [1].

TX mode	Mod	CC rate	RS code	Overall rate	Bitrate [Mbit/s]
T1	BPSK	1/2	(12,12,0)	1/2	5.6
T2	QPSK	2/3	(32,24,4)	1/2	11.2
T3	QPSK	5/6	(40,36,2)	3/4	18.5
T4	16-QAM	2/3	(64,48,8)	1/2	17
T5	16-QAM	5/6	(80,72,4)	3/4	25.2
T6	64-QAM	3/4	(108,96,6)	2/3	25.8
T7	64-QAM	5/6	(120,108,6)	3/4	30.5

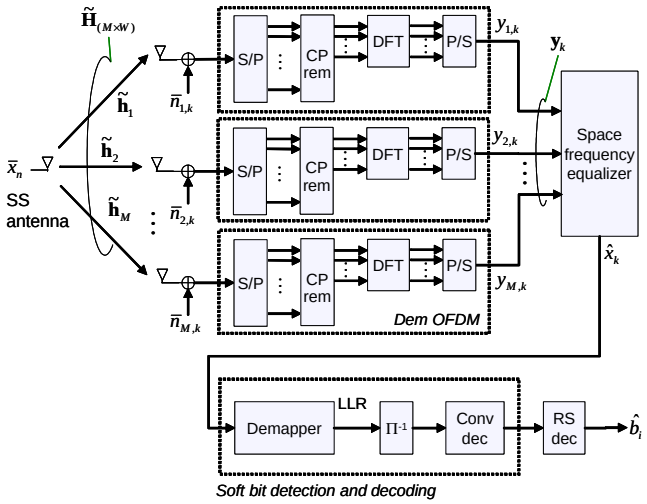

Fig. 3. Receiver baseband model.

2.1. Channel model

The $M \times K$ space-frequency matrix $\mathbf{H} = [\mathbf{h}_1 \cdots \mathbf{h}_K]$, modelling the propagation between SS_0 and BS_0, gathers the channel vectors for the K subcarriers. Its generic element $h_{m,k}$ represents the channel gain of the mth receiving antenna on the kth subcarrier. The space-frequency channel can be seen as the DFT transformation by rows of the $M \times W$ space-time channel matrix $\widetilde{\mathbf{H}}$:

$$\mathbf{H} = \widetilde{\mathbf{H}}\mathbf{F}^{\mathrm{T}}, \quad (3)$$

where $\mathbf{F}$ is the $K \times W$ DFT matrix. Its element (k, w), for $k = 1, \ldots, K$ and $w = 1, \ldots, W$, is defined as

$$F_{k,w} = \exp\left[-\frac{j2\pi}{N} n_k (w-1)\right], \quad (4)$$

with $n_k \in \{0, \ldots, N-1\}$ denoting the frequency index for the kth useful subcarrier and N the total number of subcarriers.

In our framework the channel $\widetilde{\mathbf{H}}$ is modelled by means of a space-time multipath model [5] [6], characterized by the superposition of N_p paths' contributions. The rth path is described by a

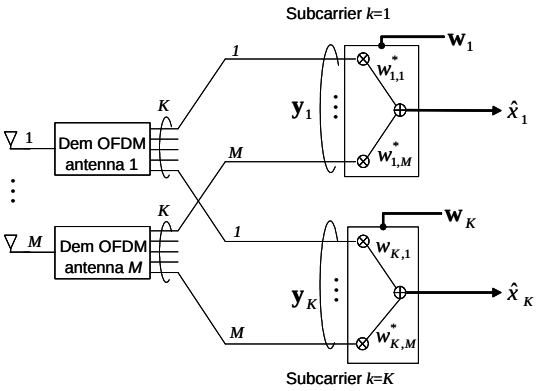

Fig. 4. Space-frequency equalizer structure based on MVDR filters.

Table 2. Relevant system parameters

Carrier frequency f_c	3.5 GHz
Bandwidth B	$8/7 \times 3.5 = 4$ MHz
Number of subcarriers N	256
Number of useful subcarriers K	192 data + 8 pilots
Number of guard-band subcarriers	28+27
Subcarrier spacing Δf	15.625 kHz
Useful symbol time T_s	64 μs
Cyclic-prefix time T_c	8 μs
OFDM symbol time T_s	72 μs
SS omnidirectional antenna gain G_T	2 dBi
BS directional antenna gain G_R	16 dBi (broadside)
Path loss exponent n	4
Noise figure	7 dB
Shadowing standard deviation σ_s	8 dB
SS maximum power $P_T^{(\max)}$	27 dBm

direction of arrival (DOA) at the receiving array (θ_r), a delay (τ_r) and a complex fading amplitude (α_r):

$$\widetilde{\mathbf{H}} = \sqrt{P^{(\mathrm{R})}} \sum_{r=1}^{N_R} \alpha_r \mathbf{a}(\theta_r)\mathbf{g}^{\mathrm{T}}(\tau_r). \tag{5}$$

The $M \times 1$ vector $\mathbf{a}(\theta_r)$ denotes the array response to the direction of arrival θ_r. For a linear array with spacing Δ_m between the mth and the $(m+1)$th antennas, the mth element of the steering vector $\mathbf{a}(\theta_r)$ is defined as

$$[\mathbf{a}(\theta_r)]_m = \exp\left(j2\pi \frac{\sin(\theta_r)}{\lambda} \sum\nolimits_{\ell=1}^{m-1} \Delta_\ell\right) \tag{6}$$

for $m = 2, \ldots, M$, while for $m = 1$ it is $[\mathbf{a}(\theta_r)]_0 = 1$. The $W \times 1$ vector $\mathbf{g}(\tau_r)$ collects the symbol-spaced samples of the waveform $g(t-\tau_r)$, that is convolution of the transmitter and receiver filter impulse responses, shifted by the delay τ_r. The path amplitudes are assumed to be uncorrelated Rice-faded, $\alpha_r \sim \mathcal{CN}(\mu_r, \sigma_r^2)$, with mean value μ_r, variance σ_r^2, Rice factor $K_r = |\mu_r|^2/\sigma_r^2$, and normalized power-delay-angle-profile $\Lambda_r = \mathrm{E}[|\alpha_r|^2]$ so that $\sum_{r=1}^{N_R} \Lambda_r = 1$. In case of non-line-of-sight (NLOS) path, K_r is set to zero and Raylegh fading is considered. $P^{(\mathrm{R})}$ is the average received power.

The multipath parameters $\{\tau_r, \Lambda_r, K_r\}_{r=1}^{N_\mathrm{R}}$ are chosen according to the Stanford University Interim (SUI) channel models [5], while the directions of arrivals $\{\vartheta_\ell\}_{\ell=1}^{N_\mathrm{R}}$ are herein modelled as uncorrelated Gaussian random variables, $\vartheta_r \sim \mathcal{N}\left(\overline{\vartheta}, \sigma_\vartheta^2\right)$, with angular spread σ_ϑ and mean direction $\overline{\vartheta}$ corresponding to the direct path SS_0-BS_0. In case of null angular spread ($\sigma_\vartheta = 0$ deg) the channel will be referred to as a no-spatial-diversity (No-SD) channel. The settings used for performance evaluation are those defined by SUI-3 and SUI-4 models, which are representative of propagation environments with, respectively, low ($\sigma_\tau = 0.26\mu s$) and moderate ($\sigma_\tau = 1.41\mu s$) delay spread (see Table 3). It is worth noticing that the temporal dispersion has a great impact on the performance of coded OFDM systems over fading channels, as frequency selectivity allows the decoder to exploit the diversity in the frequency domain. Hence, in order to better investigate the behavior of the OFDM systems, along with SUI-3 and SUI-4, we also consider two simplified fading models that can be seen as extreme cases of frequency selectivity (to be used as reference for performance evaluation):

- No frequency diversity (No-FD): null delay spread ($\tau_r = 0$, $\forall r$) or, equivalently, frequency-flat channel ($h_{m,k} = h_m \; \forall k$).
- Maximum frequency diversity degree (Max-FD): the channel gains are independent identically distributed over the K subcarriers ($h_{m,k}$ is uncorrelated over the frequency index k).

Table 3. SUI parameters.

Multipath parameter	SUI-3			SUI-4		
	$\ell = 1$	$\ell = 2$	$\ell = 3$	$\ell = 1$	$\ell = 2$	$\ell = 3$
τ_ℓ [μs]	0	0.4	0.9	0	1.5	4
P_ℓ [dB]	0	-5	-10	0	-4	-8
K_ℓ	1	0	0	0	0	0

The power $P^{(\mathrm{R})}$ received by BS_0 from SS_0 is modelled as

$$P^{(\mathrm{R})}[\mathrm{dBm}] = P^{(\mathrm{T})}[\mathrm{dBm}] + G - L(d_0) + S_0, \tag{7}$$

where $P^{(\mathrm{T})}$ denotes the transmitted power, $G = G^{(\mathrm{T})} + G^{(\mathrm{R})}$ [dB] the transmitter-receiver antenna gain, $L(d_0)$ [dB] the power loss over the distance d_0 between SS_0 and BS_0, $S_0 \sim \mathcal{N}(0, \sigma_s^2)$ the random fluctuations due to shadowing. As recommended in [2], the path-loss is modelled according to the Hata-Okamura model [7]

$$L(d) = 20\log_{10}\left(\frac{4\pi d_{\mathrm{ref}}}{\lambda}\right) + 10\gamma\log_{10}\left(\frac{d}{d_{\mathrm{ref}}}\right) + 6\log_{10}\left(\frac{f_c}{2}\right) \tag{8}$$

with λ denoting the wavelength [m], γ the path-loss exponent, d_{ref} a reference distance [m], and f_c the carrier frequency [GHz]. Notice also that $P^{(\mathrm{T})}$ is limited by the maximum power available at the SS's, i.e. $P^{(\mathrm{T})} \leq P_{\max}^{(\mathrm{T})}$. It is important to point out that the random power fluctuations described above have to be ascribed to variations of the user position. Even though our framework refers to a fixed wireless system, these fluctuations will be simulated in order to evaluate the system performance averaged over the user position within the cell.

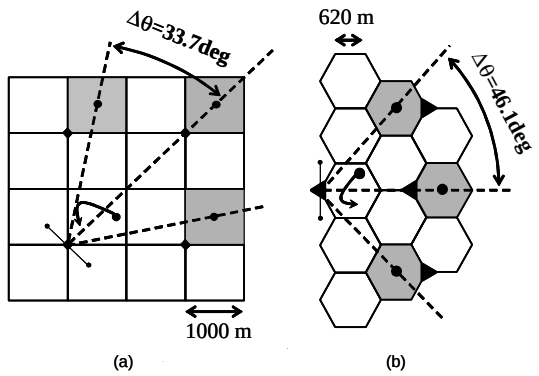

Fig. 5. Positions of the interfering cells for the considered cellular layouts: a) Square cell planning with reuse factor $F = 4$; b) Hexagonal cell planning with reuse factor $F = 3$.

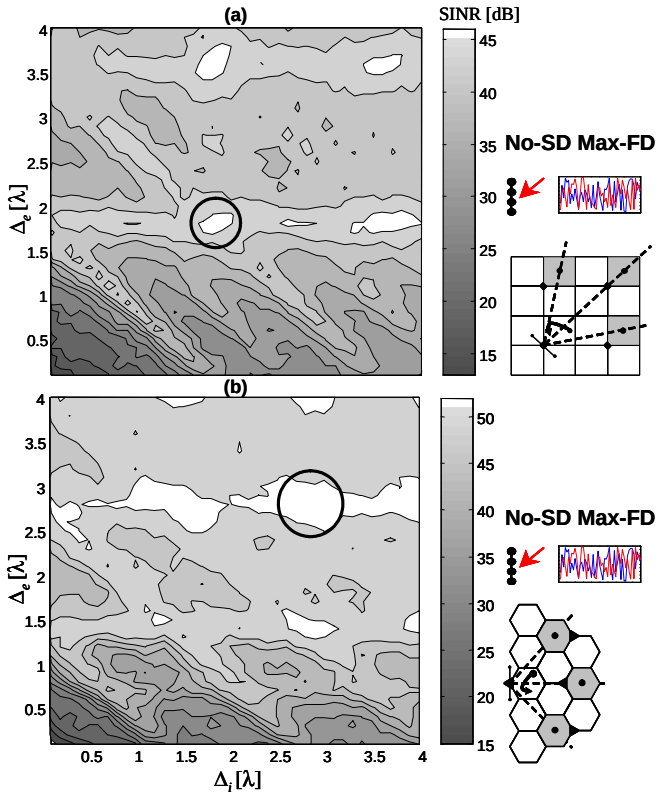

Fig. 6. SINR at the output of the MVDR filter versus antenna spacings Δ_e and Δ_i ($M = 4$) averaged with respect to fading and users positions within the cell. Fixed positions are considered for the interferers according to the square (a) and hexagonal (b) cell planning in fig. 5.

2.2. Interference model

The noise covariance $\mathbf{Q} = \mathbf{Q}_n + \mathbf{Q}_I$ is the sum of the background noise matrix $\mathbf{Q}_n = \sigma_n^2 \mathbf{I}_M$ and the contribution $\mathbf{Q}_I$ from the N_I active out-of-cell interferers. We assume that the signal from each interferer SS_i, $i = 1, \ldots, N_I$, is received by BS_0 through a multipath channel with the same characteristics as in (5). It follows that the ith interferer spatial covariance (averaged with respect to fast fading) depends on the DOA's $\{\theta_{i,r}\}_{r=1}^{N_R}$, the normalized power-angle-profile $\{\Lambda_{i,r}\}_{r=1}^{N_R}$ and the received power $P_{i0}^{(\text{R})}$, according to:

$$\mathbf{Q}_I = \sum_{i=1}^{N_I} \sqrt{P_{i0}^{(\text{R})}} \sum_{r=1}^{N_R} \Lambda_{i,r} \mathbf{a}(\theta_{i,r}) \mathbf{a}^{\text{H}}(\theta_{i,r}). \qquad (9)$$

As in (7), the received power is obtained from the power $P_i^{(\text{T})}$ transmitted by SS_i, taking into account the power loss due to propagation over the distance d_{i0} and the shadowing effect $S_{i0} \sim \mathcal{N}(0, \sigma_s^2)$ over the link SS_i-BS_0:

$$P_{i0}^{(\text{R})}[\text{dBm}] = P_i^{(\text{T})}[\text{dBm}] + G - L(d_{i0}) + S_{i0}. \qquad (10)$$

Notice that, in order to satisfy the constraint on the bit error rate (BER$\leq 10^{-6}$) at the base station BS_i, power control must be adopted in the communication between SS_i and BS_i (see fig. 1):

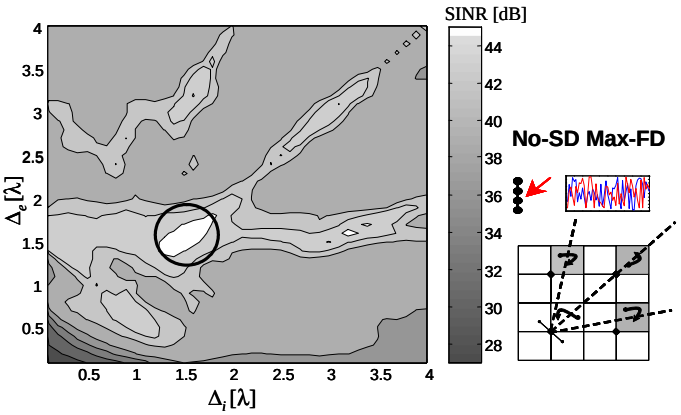

Fig. 7. SINR at the output of the MVDR filter versus antenna spacings Δ_e and Δ_i ($M = 4$) averaged with respect to uniformly distributed positions of user and interferers according to the square cell planning in fig. 5-(a).

the power $P_i^{(\text{T})}$ transmitted by SS_i is chosen so as to compensate (up to the maximum available power $P_{\max}^{(\text{T})}$) the path loss and the shadowing S_i over the distance d_i. As a consequence, the shadowing effects on the interference power $P_{i0}^{(\text{R})}$ are higher than those on the useful signal power $P^{(\text{R})}$, as they are the superposition of the two fluctuations S_i and S_{i0}. Numerical values for the system parameters defined throughout this section can be found in Table 2.

3. OPTIMAL ARRAY DESIGN

In this Section, we tackle the problem of finding optimal antenna spacings for the array deployed at the BS (in the example in fig. 1, the vector $\boldsymbol{\Delta} = [\Delta_i \ \Delta_e]^T$). Different performance metrics can be used in order to set up the optimization problems. A relevant criterion is the maximization of the ergodic capacity of the system

$$C = \text{E}[\log_2(1 + \rho_k)] \ [\text{bit/s/Hz}] \qquad (11)$$

or the average $\text{E}[\rho_k]$ of the SINR (2) at the output of the MVDR

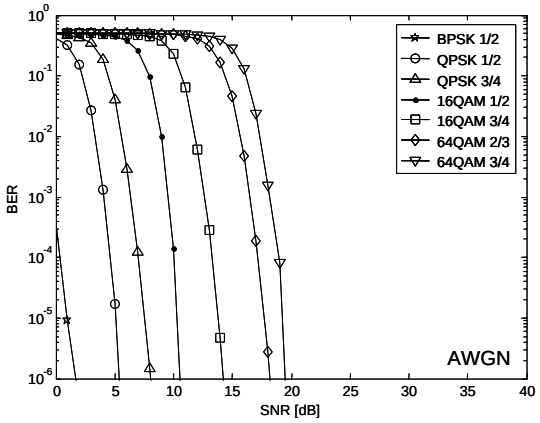

Fig. 8. BER versus SINR for all the transmission mode in AWGN.

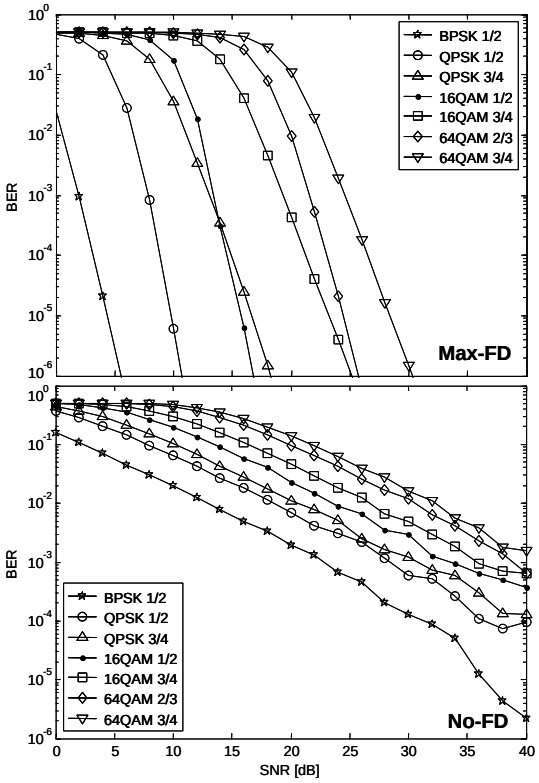

Fig. 9. BER versus SINR for all the transmission mode in Max-FD (top) and No-FD (bottom) channels.

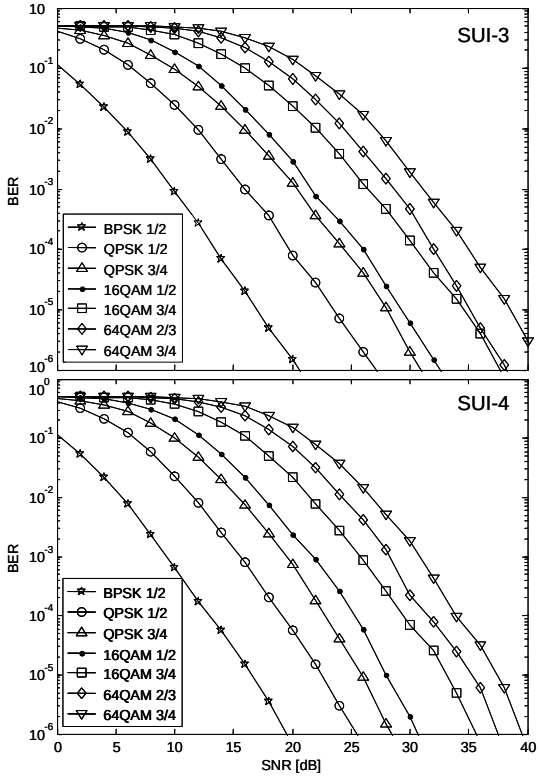

Fig. 10. BER versus SINR for all the transmission modes in SUI-3 (top) and SUI-4 (bottom) channels.

filter. Moreover, while for some static applications it might be of interest to find the optimal spacings for a fixed position of user and interferers, this is not the case in general. In fact, in many applications the position of users and interferers is not known a priori at the time of the antenna deployment, or it varies due to terminal mobility. Therefore, in such scenarios, the appropriate performance criterion has to be averaged over the expected positions of user and interferers within their cells before being optimized. In [4] the problem of maximizing the ergodic capacity has been tackled from an analytical standpoint. It was shown therein that, according to the propagation environment and the interference layout, relevant performance gains can be obtained by selecting the optimal antenna deployment as trade-off between diversity and interference mitigation.

3.1. Numerical results

We consider the two interfering scenarios in fig. 5: a square cell planning with reuse factor $F = 4$ (a) and an hexagonal cell planning with $F = 3$ (b). A symmetric array with $M = 4$ antennas is assumed at the base station BS_0. Recalling the definitions in Sec. 2.1, this first analysis is referred to a simplified channel model that assumes fading uncorrelation over the subcarriers (Max-FD) and null angular spread σ_ϑ (No-SD). Shadowing is not accounted for ($\sigma_s = 0$). The main system parameters are listed in Table 2, all terminals are assumed to transmit at maximum power $P_{\max}^{(\mathrm{T})}$.

In Fig. 6 the average SINR $\mathrm{E}[\rho_k]$ at the output of the MVDR filter is plotted in gray scale versus the external (Δ_e) and internal (Δ_i) spacings, for the two plannings in fig. 5. Exemplifying drawings on the right of the figure are used to recall the space/frequency characteristics of the considered propagation environment. For each pair (Δ_e, Δ_i), the SINR value is obtained by averaging (2) over the fading channel and the position of the user SS_0 (uniformly distributed within the cell). The interferers $\{\mathrm{SS}_i\}_{i=1}^3$ are herein placed in fixed positions as indicated in the plots on the right of the figure. The results obtained for both the square (a) and hexagonal (b) layouts show that the minimum-length array that maximizes the average SINR is uniform with $\Delta_i = \Delta_e = \Delta_{opt}$: the optimal spacing is $\Delta_{opt} = 1.81\lambda$ for the layout (a) and $\Delta_{opt} = 1.39\lambda$ for the layout (b). This result is a trade-off between interference mitigation capability (small Δ) and diversity exploitation (large Δ) and it confirms the analytical results obtained in [4] for a generic wireless system. In particular, for the scenario at hand, the optimal spacings can be found to be $\Delta_i = \Delta_e = n\Delta_{opt}$ with $\Delta_{opt} = \lambda/\sin(\Delta\theta)$. The optimal spacings are larger than the canonical $\lambda/2$ and they provide at least a SINR gain of 5dB with respect to other standard antenna deployments. Such gain can be justified by noticing that the optimal spacings introduce a certain degree of angular equivocation in the directivity function of the array so that the interferers are grouped together along an unique direction. The wave numbers associated to the DOAs of the interferers SS_1 and SS_3 are indeed $\omega_{1,3} = 2\pi\frac{\Delta}{\lambda}\sin\theta_i = \pm 2\pi n$ and coincide with that of the broadside interferer SS_2 ($\omega_2 = 0$). This effects renders interference mitigation more effective.

In fig. 7 the assumption of fixed interferers is removed, the SINR is averaged with respect to the positions of both user and interferers within the respective cells of the square cell planning in fig. 5-

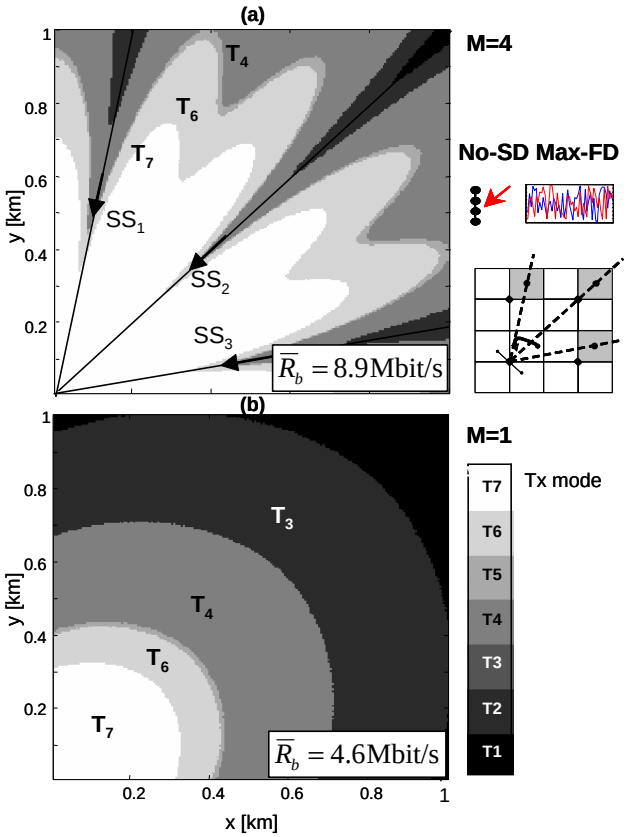

Fig. 11. Coverage for a square planning: a) optimized array receiver with $M = 4$ antennas (the arrows indicate the directions of arrival of the interferers); b) single-antenna receiver ($M = 1$).

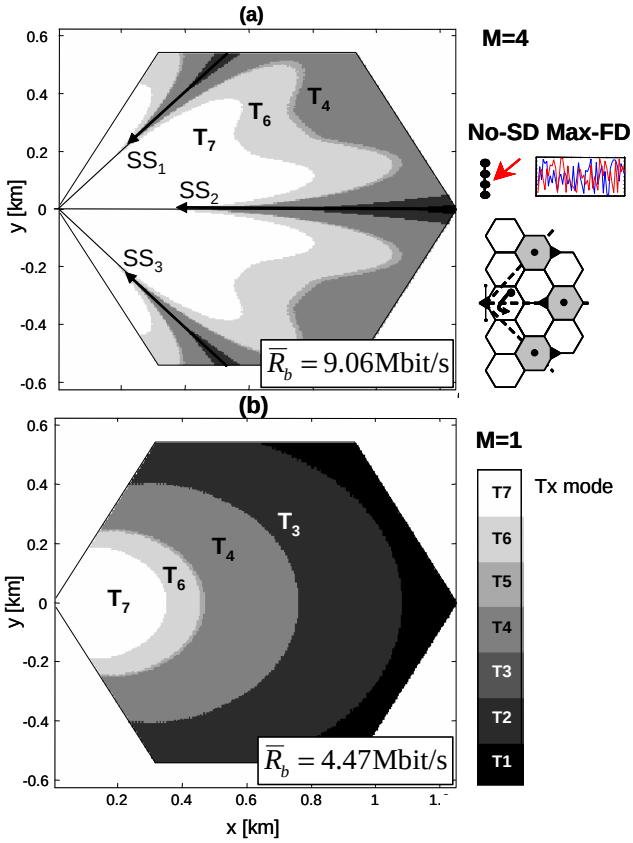

Fig. 12. Coverage for an hexagonal planning: a) optimized array receiver with $M = 4$ antennas (the arrows indicate the directions of arrival of the interferers); b) single-antenna receiver ($M = 1$).

(a). In this case the optimal solution turns out to be $\Delta_i = \Delta_e = \lambda/\sin(\Delta\theta) = 1.81\lambda$ and the performance gain with respect to standard antenna deployment reduces to 2dB.

4. THROUGHPUT EVALUATION

In this section we compare the average throughput provided by the optimized array with inter-element spacing Δ_{opt} with that obtained by a conventional array designed for beamforming usage. The performance gain of the optimized array is evaluated for both the cellular layouts in fig. 5, for $M = 1 \div 4$, channel models as defined in Section 2.1 and for fixed interferers at the center of their respective cells. We recall that the inter-element spacing that maximizes the beamforming resolution under the non-alias constraint is $\Delta_m = \lambda/[2\sin(\theta_{\max})]$ where $\theta_{\max}$ is the largest DOA admissible for the considered cellular layout. For the plannings in fig. 5 it is: (a) $\theta_{\max} = \pi/4$ and $\Delta_m = 0.71\lambda$; (b) $\theta_{\max} = \pi/4$ and $\Delta_m = 0.58\lambda$.

The average throughput for the overall cell is evaluated in the following way. For each position of the user SS_0, the SINR at the output of the MVDR filter is averaged with respect to the channel, the noise and the interference. Next, for each average SINR value, using pre-evaluated BER versus SINR average performance measurements (see fig. 8, 9 and 10 for $M = 1$), we select the best transmission mode T_i from the available set to satisfy the constraint $BER \leq 10^{-6}$ and provide the largest bit-rate. This allows to obtain a coverage map for all transmission modes $\{T_i\}_{i=1}^{7}$, as those exemplified in figures 11-12 for the channel model Max-FD with null angular spread (No-SD). These examples refer to the square (fig. 11) and hexagonal (fig. 12) layouts, with optimized antenna array composed of $M = 4$ antennas (top figure) or with single antenna (bottom figure). Similar coverage maps have been derived for the other propagation environments using BER vs. SINR average performances.

Once the coverage maps have been obtained, the average throughput $\bar{R}_b$ [bit/s] for the overall cell can be evaluated through a weighted average of the throughputs $\{R_{b,i}\}_{i=1}^{7}$ associated to the different transmission modes $\{T_i\}_{i=1}^{7}$, using as weighting factors the (normalized) areas where the modes are supported $\{A_i\}_{i=1}^{7}$:

$$\bar{R}_b = \sum_{i=1}^{7} A_i R_{b,i}.$$

The throughput $R_{b,i}$ of the ith transmission mode is calculated by taking into account both the cyclic-prefix loss and the fact that only $K - 8 = 192$ out of $N = 256$ subcarriers are used for data transmission (see Table 2):

$$R_{b,i} = \frac{(K-8)N_{b,i}R_{c,i} - 8}{T_s}, \qquad (12)$$

where $N_{b,i}$ and $R_{c,i}$ are, respectively, the number of bits per sym-

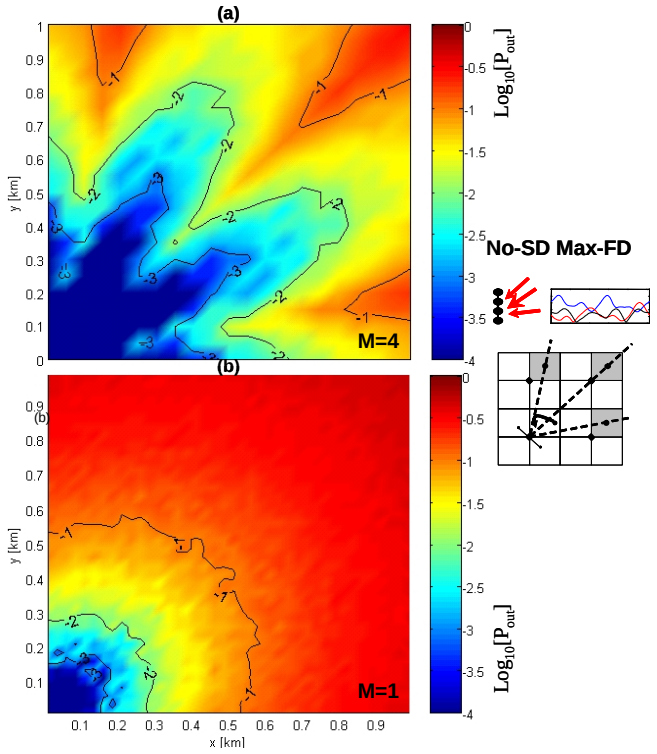

Fig. 13. Outage probability versus the user position for a square cell planning: a) optimized uniform array receiver with $M = 4$; b) single-antenna receiver.

bol and the coding rate for the transmission mode T_i, while T_s is the OFDM symbol duration including the cyclic prefix. Notice that, during each symbol, the message sequence is padded at the end with 8 information bits so that the convolutional encoder returns to a known state after having encoded the message.

The average throughput has been derived by the procedure above for both the square and hexagonal layout, using an antenna array of $M = 1 \div 4$ antennas at the BS, with antenna spacing Δ_{opt} or Δ_m. The numerical results are summarized in the tables in fig. 14 and 15, including both the case of omnidirectional antennas (rows $1 \div 4$) and directional antennas (rows $5 \div 8$). Each column refers to a different channel model: no frequency diversity and null angular spread (No-FD No-SD, column 1); SUI-3 with null angular spread (SUI-3 No-SD, column 2); SUI-4 with null angular spread (SUI-4 No-SD, column 3); maximum frequency diversity with null angular spread (Max-FD No-SD, column 4); no frequency diversity with angular spread $\sigma_\theta = 5$deg (No-FD SD, column 5). For instance, the results $\bar{R}_b = 8.9$Mbit/s (for $M = 4$) and $\bar{R}_b = 4.6$Mbit/s (for $M = 1$) obtained in fig. 11 can be easily found in the top part of fig. 14 (for omnidirectional antennas), in the column referring to No-FD No-SD channel, with antenna spacing Δ_{opt}. As expected, from the exploitation of diversity either in space or in frequency, the overall system throughput may be considerably enhanced. In addition, for the square cell planning, an optimized array is shown to provide substantial throughput improvements with respect to the conventional beamforming-oriented array. On the other hand, for the hexagonal cell planning, due to the reduced frequency reuse factor F that increases the co-channel average interference level, substantially lower throughput improvement is observed.

5. OUTAGE PROBABILITY ANALYSIS

In this section, the impact of SINR fluctuations due to fading and shadowing is studied by evaluating the outage probability for a fixed transmission mode (T_6). An outage event occurs whenever the system BER P_b exceeds a certain threshold $\bar{P}_b$ and the outage probability is thus defined as $P_{out} = pr(P_b > \bar{P}_{out})$.

Fig. 13 shows the outage probability versus the user position within its cell for an optimized uniform $M = 4$ antenna array (fig. 13-a) and for the single antenna case (fig. 13-b). The square cell planning is considered with fixed interferers positions. Moreover, the SUI-3 channel model is simulated with angular spread $\sigma_\vartheta = 5$ deg and power of the lognormal density of shadowing $\sigma_s = 8$dB. The analysis in terms of outage probability yields similar conclusions to the investigation of throughput coverage, lending evidence to the performance benefits of a multiantenna receiver with optimized spacings.

6. CONCLUSION

Optimal deployment of an antenna array at the base station of a cellular system is the result of a trade-off between diversity and interference-rejection capability. In this paper, the performance gains of an optimized antenna deployment are investigated in terms of system throughput for a WiMAX-compliant uplink. Thorough simulation results are presented for square and hexagonal cell layouts and a wide range of propagation scenarios. The main conclusion is that relevant benefits are obtained by letting the antenna spacings be larger than the conventional $\lambda/2$. Therefore, throughput maximization comes at the price of a reduced effectiveness of the array for applications that require unambiguous determination of the propagation angles (e.g., localization). An extension of the analysis presented in this paper is in progress for mobile OFDMA systems conforming to the IEEE 802.16e standard.

7. REFERENCES

[1] A. Ghosh, D.R Wolter, J. G. Andrews, R. Chen, "Broadband wireless access with WiMAX/802.16: current performance benchmarks and future potential," IEEE Communications Magazine, Vol. 43, No. 2, pp. 129-136, Feb. 2005.

[2] IEEE Std 802.16^{TM}-2004, "802.16^{TM} IEEE standard for local and metropolitan area networks Part 16: Air interface for fixed broadband wireless access systems," October 2004.

[3] IEEE P802.16-2004/Cor1/D5 (Draft Corrigendum to IEEE Std 802.16-2004), "Corrigendum to IEEE standard for local and metropolitan area networks - Part 16: Air interface for fixed broadband wireless access systems," Sep. 2005.

[4] S. Savazzi, O. Simeone, and U. Spagnolini, "Optimal design of linear arrays in a TDMA cellular system with Gaussian interference," Proc. IEEE SPAWC, pp. 485-489, June 2005.

[5] IEEE 802.16.3c-01/53, IEEE 802.16 Broadband Wireless Access Working Group, "Simulating the SUI channel models," April 2004.

[6] A. Abdi and M. Kaveh, "A space-time correlation model for multielement antenna systems in mobile fading channels," J. Select. areas Commun., Vol. 20, No. 3, pp. 550-560, April 2002.

[7] A. Goldsmith, Wireless communications, Cambridge University Press, 2005.

[8] H. L. Van Trees, Optimum array processing, Wiley, 2002.

Channel / Antennas	No-FD No-SD		SUI-3 No-SD		SUI-4 No-SD		Max-FD No-SD		No-FD SD.	
⊙	Δ_m	Δ_{opt}	Δ_m	Δ_{opt}	Δ_m	Δ_{opt}	Δ_m	Δ_{opt}	Δ_m	Δ_{opt}
M = 1	0.19	0.19	0.96	0.96	1.15	1.15	4.61	**4.61**	0.19	0.19
M = 2	0.32	0.42	1.50	1.98	1.80	2.36	5.94	6.70	1.14	1.81
M = 3	0.39	0.61	1.89	2.93	2.26	3.41	6.80	8.05	1.94	3.75
M = 4	0.53	0.77	2.53	3.47	2.99	4.06	7.64	**8.90**	2.93	5.27
ρ	Δ_m	Δ_{opt}	Δ_m	Δ_{opt}	Δ_m	Δ_{opt}	Δ_m	Δ_{opt}	Δ_m	Δ_{opt}
M = 1	0.27	0.27	1.31	1.31	1.57	1.57	5.50	5.50	0.27	0.27
M = 2	0.39	0.58	1.92	2.71	2.29	3.18	6.87	7.81	1.50	2.45
M = 3	0.51	1.09	2.47	4.50	2.96	5.21	7.67	10.12	2.55	4.85
M = 4	0.70	1.49	3.25	5.52	3.81	6.27	8.67	10.63	3.76	6.51

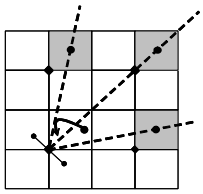

Fig. 14. Average throughput [Mbit/s] for the uplink of the square cellular planning on the right, with an antenna array of M elements at the BS and a single antenna at each SS. The number of receiving antennas M ranges from 1 to 4. The inter-element spacing at the BS array is the conventional one used for beamforming (Δ_m) or the optimized one for throughput maximization (Δ_{opt}). The transmitting antenna at each SS is omnidirectional (top section of the Table) or directional (bottom section). Each column refers to a different channel model: no frequency diversity and null angular spread (No-FD No-SD, column 1); SUI-3 with null angular spread (SUI-3 No-SD, column 2); SUI-4 with null angular spread (SUI-4 No-SD, column 3); maximum frequency diversity with null angular spread (Max-FD No-SD, column 4); no frequency diversity with angular spread $\sigma_\theta = 5$deg (No-FD SD, column 5). Bold values are obtained from the simulation in figure 11.

Channel / Antennas	No-FD No-SD		SUI-3 No-SD		SUI-4 No-SD		Max-FD No-SD		No-FD SD	
⊙	Δ_m	Δ_{opt}	Δ_m	Δ_{opt}	Δ_m	Δ_{opt}	Δ_m	Δ_{opt}	Δ_m	Δ_{opt}
M = 1	0.21	0.21	0.95	0.95	1.13	1.13	4.47	**4.47**	0.20	0.20
M = 2	0.29	0.39	1.36	1.88	1.61	2.23	5.56	6.60	0.96	1.60
M = 3	0.39	0.61	1.86	2.87	2.23	3.37	6.70	8.00	1.60	3.14
M = 4	0.52	0.82	2.45	3.63	2.91	4.22	7.55	**9.06**	2.37	4.54
ρ	Δ_m	Δ_{opt}	Δ_m	Δ_{opt}	Δ_m	Δ_{opt}	Δ_m	Δ_{opt}	Δ_m	Δ_{opt}
M = 1	0.30	0.20	1.38	1.38	1.64	1.64	5.63	5.63	0.29	0.29
M = 2	1.16	1.57	4.34	5.53	5.00	6.28	9.74	10.66	2.23	2.56
M = 3	2.01	2.18	6.60	6.98	7.31	7.68	11.08	11.22	4.26	5.14
M = 4	2.53	2.63	7.73	7.78	8.42	8.49	11.36	11.40	5.94	7.07

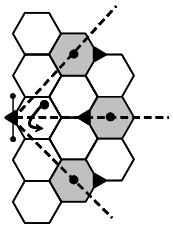

Fig. 15. Average throughput [Mbit/s] for the uplink of the hexagonal cellular planning on the right, with an antenna array of M elements at the BS and a single antenna at each SS. The number of receiving antennas M ranges from 1 to 4. The inter-element spacing at the BS array is the conventional one used for beamforming (Δ_m) or the optimized one for throughput maximization (Δ_{opt}). The transmitting antenna at each SS is omnidirectional (top section of the Table) or directional (bottom section). Each column refers to a different channel model: no frequency diversity and null angular spread (No-FD No-SD, column 1); SUI-3 with null angular spread (SUI-3 No-SD, column 2); SUI-4 with null angular spread (SUI-4 No-SD, column 3); maximum frequency diversity with null angular spread (Max-FD No-SD, column 4); no frequency diversity with angular spread $\sigma_\theta = 5$deg (No-FD SD, column 5). Bold values are obtained from the simulation in figure 12.